

Spurious-free analysis of two-dimensional low-loss metallic gratings

This content has been downloaded from IOPscience. Please scroll down to see the full text.

2016 J. Opt. 18 035001

(<http://iopscience.iop.org/2040-8986/18/3/035001>)

View [the table of contents for this issue](#), or go to the [journal homepage](#) for more

Download details:

IP Address: 129.97.58.73

This content was downloaded on 06/02/2016 at 14:30

Please note that [terms and conditions apply](#).

Spurious-free analysis of two-dimensional low-loss metallic gratings

Hoda Fadakar¹, Abolghasem Zeidaabadi Nezhad¹, Amir Borji² and Mahmoud Shahabadi³

¹Department of Electrical and Computer Engineering, Isfahan University of Technology, Isfahan, Iran

²Department of Electrical Engineering, Sharif University of Technology, Tehran, Iran

³School of Electrical and Computer Engineering, University of Tehran, Tehran, Iran

E-mail: hoda.fadakar@gmail.com

Received 17 October 2015, revised 15 December 2015

Accepted for publication 23 December 2015

Published 4 February 2016



CrossMark

Abstract

Transmission line formulation is used to analyze two-dimensional low-loss metallic gratings at optical frequencies when plasmonic waves propagate in the structure. This method, like the Fourier modal method, suffers from numerical instabilities when applied to such structures. A systematic approach to avoid these instabilities is presented. These numerical artifacts are attributed to the violation of Li's inverse rule and the appearance of higher-order spurious modes. In this paper, a new approach is proposed to identify and to greatly reduce the effect of these spurious modes based on the accuracy by which these modes are satisfying the conservation of momentum. Furthermore, the proposed scheme conserves power and improves the convergence, i.e., reduces the required truncation order.

Keywords: metallic grating, transmission line formulation, numerical instabilities, spurious modes

(Some figures may appear in colour only in the online journal)

1. Introduction

Multilayered structures involving periodic metallic gratings have attracted considerable attention in recent years due to their numerous applications at optical and terahertz frequencies [1–6]. Fourier-based methods, such as the Fourier modal method (FMM), also known as rigorous coupled-wave analysis [7], and transmission line formulation (TLF) [8, 9] are among common tools for modeling these grating structures. Applying Li's inverse rule [10] enables these methods to appropriately analyze almost any grating at optical frequencies. However, the methods still face difficulties when used to analyze low-loss and lossless plasmonic gratings [11, 12].

Transverse field components are usually singular over sharp corners and edges. In lossless plasmonic structures, these singularities are more pronounced due to the sign change in permittivities of the involved materials, namely, metals and dielectrics. In [12], field singularities were classified as regular and irregular, and a simple criterion was established to distinguish the type of singularity for a right-

angled edge. Furthermore, it was shown that any method using a Fourier series fails to correctly represent the electric field components transverse to an edge when irregular singularity is present [12]. This type of singularity only occurs if there are edges containing a lossless metal. On the other hand, FMM as well as TLF suffer from another type of numerical instability when applied to metallic gratings in TM polarization that is independent of field singularity at the edges. These numerical artifacts are associated with inaccuracies in computing the eigenmodes. In [13–15], the numerical instability of the FMM was improved by enhancing the spatial resolution of the method at discontinuities. In [11], the numerical instabilities of the FMM were attributed to the ill-conditioned matrices to be diagonalized. The authors of [11] introduced artificial metal losses and applied a two-step truncation of matrices in order to diminish these instabilities. In [16], it was shown that, by increasing the number of spatial harmonics used in the FM series, the numerical artifacts are reduced greatly. These numerical instabilities were shown to be due to nonuniform convergence of the truncated matrix eigenvalue problem inside the grating region [16]. In [17], this problem

has been associated with the computation of eigenmodes after truncating the infinite-dimensional matrices of coefficients in the FMM [17]. As a result, spurious grating modes appear among true (but approximate) eigenmodes of the structure [17]. Thus, a filtering mechanism was proposed to suppress these unwanted modes and to eliminate the numerical instabilities.

With regard to the convergence problem due to irregular field singularity at the edges, it must be stressed that this convergence problem exists even if the grating modes are computed by the exact modal method that is free of spurious modes. In [18, 19], a rectangular truncation of matrices, instead of a square truncation, was proposed to mitigate the convergence problem for a structure showing irregular field singularities. For $M + 1$ grating modes, $2M + 1$ Fourier coefficients were retained, and a minimum least squares method was applied to obtain the unknown coefficients. Since the above rectangular truncation may underestimate the total power of the scattered field, an energy conservation constraint was imposed on the solution [19]. In [20], it was suggested to replace the lossless metal–dielectric right-angled edges by a medium with a gradually varying refractive index so as to remove the irregular field singularities. Also, coordinate transformation was used to increase the spatial resolution of the approximate medium and to improve the convergence.

In all the above cases, only one-dimensional (1D) metallic gratings have been considered. In two-dimensional (2D) periodic gratings, when the total number of spatial harmonics is increased, the Fourier-based methods become time consuming and encounter exhaustion of dynamic memory. Therefore, any attempt to improve the numerical efficiency is of practical significance. In this paper, the problem of unpredictable instabilities in 2D periodic metallic gratings is studied by using the TLF. It will be shown that, similar to the 1D case considered in [17], the cause of the instabilities is the appearance of spurious modes (eigenvalues). As the truncation order increases, these spurious eigenvalues can never be an approximation of the true eigenvalues of the underlying boundary-value problem. However, in contrast to 1D periodic gratings, there is no analytical method to be used as a reference to recognize these spurious modes. Moreover, in 2D metallic gratings, the real-valued spurious modes occur among the real-valued correct modes, which makes their identification much more difficult. Thus, in addition to a set of spurious mode detection criteria that was proposed in [17] for 1D metallic gratings, other criteria are required to specify them more easily.

In this paper, a criterion will be introduced that is used to sort the eigenvalues in the order of their accuracy so that the detection of the spurious modes of 2D metallic gratings becomes straightforward. To verify the correctness of the introduced criterion, the 1D grating structure considered in [11, 16, 17] is reinvestigated. Using the proposed error criterion and knowing the properties of the spurious modes, all spurious modes in 1D and 2D metallic gratings can be identified, and their effect can be reduced significantly without violating the power balance. As a result, the convergence

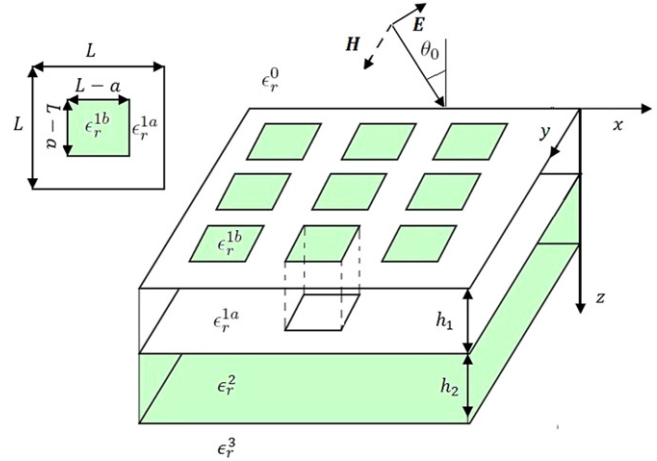


Figure 1. A typical multilayered structure containing a 2D square grating ($L_x = L_y = L$).

is also highly improved, and only a small number of Fourier expansion coefficients are required.

2. Transmission line formulation

In this section, a full-wave analysis of multilayered periodic structures using the TLF will be reviewed briefly. In this method, first, the fields in each layer are represented by their Fourier expansion and are modeled with a network of coupled multiple transmission lines, each representing a mode. Then, the necessary boundary conditions, namely, the continuity of line voltages and currents on the boundaries, are enforced, and a matrix eigenvalue problem is obtained.

A typical planar multilayered structure that includes a periodic grating is shown in figure 1. Considering the periodicity of the medium on the xy plane, the electric and magnetic fields are satisfied by the Bloch–Floquet boundary conditions, and, in each layer of the structure, these fields can be represented by the following pseudo-Fourier series:

$$\mathbf{E}_i(\mathbf{r}) = \lim_{M,N \rightarrow \infty} \sum_{m=-M}^M \sum_{n=-N}^N \mathbf{E}_{i;m,n}(z) e^{-j(\alpha_m x + \beta_n y)}, \quad (1)$$

$$\mathbf{H}_i(\mathbf{r}) = \lim_{M,N \rightarrow \infty} \sum_{m=-M}^M \sum_{n=-N}^N \mathbf{H}_{i;m,n}(z) e^{-j(\alpha_m x + \beta_n y)}, \quad (2)$$

where $\alpha_m = 2m\pi/L_x + k_x$, $\beta_n = 2n\pi/L_y + k_y$, and $i = 0, 1, 2, \dots, \mathbb{I} + 1$ is the layer index. L_x and L_y are spatial periods in the \hat{x} and \hat{y} directions, respectively, and k_x and k_y are fundamental transverse wavenumbers. Each Cartesian component of $\mathbf{E}_{i;m,n}(z)$ is represented in a single-column matrix denoted by $[E_{xi}(z)]$ in which, for instance, the entries are $E_{xi;m,n}(z)$.

The Maxwell curl equations, after applying the above matrix representation of the fields and eliminating the matrices $[E_{zi}]$ and $[H_{zi}]$, result in

$$\frac{d}{dz} \begin{bmatrix} [E_{xi}] \\ [E_{yi}] \end{bmatrix} = -j\omega [L_i] \begin{bmatrix} [H_{yi}] \\ -[H_{xi}] \end{bmatrix}, \quad (3)$$

$$\frac{d}{dz} \begin{pmatrix} [H_{yi}] \\ -[H_{xi}] \end{pmatrix} = -j\omega [C_i] \begin{pmatrix} [E_{xi}] \\ [E_{yi}] \end{pmatrix}, \quad (4)$$

where the square matrices $[L_i]$ and $[C_i]$ are of $2K \times 2K$ dimension, $K = (2M + 1) \times (2N + 1)$, and are given by [8]

$$[L_i] = \mu_0 \begin{bmatrix} 1 - [\bar{\alpha}][\vec{N}_i^2]^{-1}[\bar{\alpha}] & -[\bar{\alpha}][\vec{N}_i^2]^{-1}[\bar{\beta}] \\ -[\bar{\beta}][\vec{N}_i^2]^{-1}[\bar{\alpha}] & 1 - [\bar{\beta}][\vec{N}_i^2]^{-1}[\bar{\beta}] \end{bmatrix}, \quad (5)$$

$$[C_i] = \epsilon_0 \begin{bmatrix} \left[\left[\vec{N}_i^2 \right] \right] - [\bar{\beta}]^2 & [\bar{\beta}][\bar{\alpha}] \\ [\bar{\alpha}][\bar{\beta}] & \left[\left[\vec{N}_i^2 \right] \right] - [\bar{\alpha}]^2 \end{bmatrix}. \quad (6)$$

In (5) and (6), $1 = 1_{K \times K}$ is the identity matrix, and $[\bar{\alpha}] = [\alpha]/k_0$ and $[\bar{\beta}] = [\beta]/k_0$ are diagonal matrices where $k_0 = \omega\sqrt{\mu_0\epsilon_0}$. The diagonal matrices $[\alpha]$ and $[\beta]$ are defined by [8]

$$[\alpha] = \begin{bmatrix} \alpha_{m_1} & 0 & \dots & 0 \\ 0 & \alpha_{m_2} & \dots & 0 \\ \vdots & \vdots & \ddots & \vdots \\ 0 & 0 & \dots & \alpha_{m_K} \end{bmatrix}, \quad (7)$$

$$[\beta] = \begin{bmatrix} \beta_{n_1} & 0 & \dots & 0 \\ 0 & \beta_{n_2} & \dots & 0 \\ \vdots & \vdots & \ddots & \vdots \\ 0 & 0 & \dots & \beta_{n_K} \end{bmatrix}. \quad (8)$$

The $[\vec{N}_i^2]$ matrix contains the Fourier series expansion coefficients $\epsilon_{m,n}^i(z)$ of the relative permittivity $\epsilon_r^i(\mathbf{r})$ of layer i . These coefficients are given by

$$\epsilon_{m,n}^i(z) = \frac{1}{L_x L_y} \int_0^{L_x} \int_0^{L_y} \epsilon_r^i(\mathbf{r}) e^{j\left(\frac{2m\pi}{L_x}x + \frac{2n\pi}{L_y}y\right)} dx dy. \quad (9)$$

Matrices $[\vec{N}_i^2]$ ($[\vec{N}_i^2]$) are computed by applying Li's inverse rule with respect to $x(y)$ and then applying Laurent's rule in the $y(x)$ direction [21].

It is apparent that (3) and (4) resemble the telegraphers equation for a multiconductor transmission line system if $([E_{xi}], [E_{yi}])^T$ and $([H_{yi}], -[H_{xi}])^T$ are interpreted as line voltages and currents, respectively [8]. The solution to this system of first-order differential equations for a given $[L_i]$ and $[C_i]$ is in the form of exponential functions. As shown in [8], the following eigenvalue equation can be obtained from (3) and (4):

$$\{\omega^2 [L_i][C_i] - (k_{z\kappa}^i)^2 [1]\} [p_\kappa^i] = 0, \quad (10)$$

where $(k_{z\kappa}^i)^2$ is an eigenvalue of $\{\omega^2 [L_i][C_i]\}$ and $[p_\kappa^i]$ is the corresponding normalized eigenvector ($\kappa = 1, 2, 3, \dots, 2K$). When taking the square root of $(k_{z\kappa}^i)^2$, we must choose the branch for which $\Im\{k_{z\kappa}^i\} \leq 0$ in order to have a proper decay for each mode. Having determined all $k_{z\kappa}^i$, the complete solution for $[V_i(z)]$ in each layer of figure 1 is expressed as

$$[V_i(z)] = \sum_{\kappa=1}^{2K} (\tilde{V}_{i\kappa}^+ e^{-jk_{z\kappa}^i z} + \tilde{V}_{i\kappa}^- e^{-jk_{z\kappa}^i (h_i - z)}) [p_\kappa^i], \quad (11)$$

where $\tilde{V}_{i\kappa}^+$ and $\tilde{V}_{i\kappa}^-$ are the complex voltage amplitudes of the κ th upward and downward waves, respectively, in the i th layer. Equation (11) can be written in the following matrix form:

$$[V_i(z)] = [P^i][\tilde{V}_i(z)], \quad (12)$$

in which

$$[P^i] = \{[p_1^i] \dots [p_\kappa^i] [p_{\kappa+1}^i] \dots [p_{2K}^i]\} \quad (13)$$

is a $2K \times 2K$ matrix and $[\tilde{V}_i(z)]$ is a vector containing the terms in the parentheses of (11). Similarly, $[I_i(z)]$ is given by

$$[I_i(z)] = \sum_{\kappa=1}^{2K} (\tilde{I}_{i\kappa}^+ e^{-jk_{z\kappa}^i z} - \tilde{I}_{i\kappa}^- e^{-jk_{z\kappa}^i (h_i - z)}) [q_\kappa^i], \quad (14)$$

or

$$[I_i(z)] = [Q^i][\tilde{I}_i(z)], \quad (15)$$

in which

$$[Q^i] = \{\dots [q_\kappa^i] [q_{\kappa+1}^i] \dots\} = \omega [C_i][P^i][k_{z\kappa}^i]^{-1}. \quad (16)$$

Here, $[k_{z\kappa}^i]$ is a diagonal matrix having $k_{z\kappa}^i$ as its diagonal elements.

In the case of the 1D grating, TM^z and TE^z polarizations are decoupled. The TM^z polarization contains E_z , E_x , and H_y if the structure is periodic along the x direction and uniform along y ($\partial/\partial y = 0$). Therefore, $[E_{xi}(z)]$ and $[H_{yi}(z)]$, respectively, are the voltages and currents of the equivalent transmission-line network, and $[L_i]$ and $[C_i]$ matrices are obtained from the following equations:

$$\begin{cases} [L_i] = \mu_0 (\mathbf{I} - [\bar{\alpha}][\vec{N}_i^2(z)]^{-1}[\bar{\alpha}]), \\ [C_i] = \epsilon_0 \left[\frac{1}{\vec{N}_i^2(z)} \right]^{-1}, \end{cases} \quad (17)$$

where $\left[\frac{1}{\vec{N}_i^2(z)} \right]$ is a Toeplitz matrix that contains Fourier coefficients of $1/\epsilon_r^i(\mathbf{r})$. So far, the transverse field components of each layer are represented by $[V_i]$ and $[I_i]$ vectors. In the next step, the equivalent networks of the layers are connected at their boundaries to enforce the boundary conditions, which is the continuity of the tangential field components. Therefore, all unknown voltage and current vectors can be determined after knowing the voltage and the current vectors of the incident plane wave and discarding all the reflected wave components in the last semi-infinite layer ($i = \mathbb{I} + 1$) [9].

3. Identification and suppression of spurious modes

The method of TLF suffers from instabilities when used to analyze low-loss metallic gratings at optical frequencies. In particular, when these structures are illuminated by a TM polarized plane wave, surface plasmon polaritons (SPP) can propagate at metal-dielectric interfaces. The plasmonic waves are highly confined to the interface and make the numerical modeling of these structures more challenging. As mentioned

in [17] and shown here, these numerical instabilities are due to spurious modes. In the following, physical interpretation of TLF will be discussed and, then, by utilizing this physical interpretation a criterion to sort the modes in the order of their numerical accuracy will be given. In addition, an approach used to suppress the effect of these spurious modes will be discussed.

3.1. Physical interpretation of TLF

According to (12) and (15), each layer of the structure can be modeled by two equivalent networks of transmission lines whose voltages and currents are given by $\{[V_i], [I_i]\}$ and $\{[\tilde{V}_i], [\tilde{I}_i]\}$.

$\{[V_i], [I_i]\}$ represent transverse field components in each layer. In this network, all transmission lines are coupled mutually at layer interfaces, and the characteristic impedance matrix of the network is defined by

$$[Z_c^i]^2 = [L_i][C_i]^{-1}. \quad (18)$$

$[P^i]$ and $[Q^i]$ represent linear transformations that transform the above network of coupled transmission lines into an equivalent form characterized by $\{[\tilde{V}_i], [\tilde{I}_i]\}$ in which all transmission lines are decoupled. The reason is that, if we use $[P^i]$ to change the basis of the linear space, the matrix representation of the operator $(\omega^2 [L_i][C_i])$ becomes a diagonal matrix with $(k_z^i)^2$ as its diagonal elements,

$$[k_z^i]^2 = [P^i]^{-1}(\omega^2 [L_i][C_i])[P^i]. \quad (19)$$

In fact, the new basis for the linear space is the set of eigenvectors of $(\omega^2 [L_i][C_i])$. In the new basis, the voltage vector is represented by $[\tilde{V}_i(z)]$, and transmission lines are decoupled such that the characteristic impedance of each line is 1. In other words, each line has equal inductance and capacitance per unit length $L_\kappa = C_\kappa = k_{z\kappa}^i/\omega$ and $Z_{0\kappa} = \sqrt{(L_\kappa/C_\kappa)} = 1$. Therefore, the characteristic impedance matrix of the network is the identity matrix $[\tilde{Z}_c^i] = 1_{K \times K}$.

3.2. Accuracy of the modes

We require a criterion that enables us to identify the spurious modes, especially, in 2D metallic gratings where these modes may not be far from the correct ones. Here, we propose the use of conservation of momentum,

$$\alpha^2 + \beta^2 + k_z^2 = \epsilon_r k_0^2, \quad (20)$$

which is, in fact, equivalent to satisfying the Helmholtz equation as a criterion for evaluating the accuracy of the modes. Physically, in a homogeneous layer, $[P^i]$ is the identity matrix, and the two networks characterized by $\{[V_i], [I_i]\}$ and $\{[\tilde{V}_i], [\tilde{I}_i]\}$ are identical. Thus, the behavior of each Floquet mode along the z direction is determined by one specific (k_z^i) . However, in an inhomogeneous layer, the voltage of each transmission line designated by $[V_i]$ (the Floquet mode) is a linear combination of $[\tilde{V}_i]$ or, equivalently, a linear combination of plane waves with different (k_z^i) (as shown in (11)). In

fact, in the grating layer, the transverse field of each Floquet mode $(\mathbf{E}_{i,m,n}(z))$ in (1) is a complicated function of z that can be expressed by a superposition of plane waves. In the network characterized by $\{[V_i], [I_i]\}$, spatial derivatives of transverse fields with respect to x and y are equivalent to multiplying their corresponding voltages/currents by $-jk_0[\tilde{\alpha}]$ and $-jk_0[\tilde{\beta}]$, respectively. Furthermore, the second-order derivative of voltages with respect to z is equal to $\frac{\partial^2}{\partial z^2}[V_i(z)] = (\omega^2 [L_i][C_i])[V_i(z)]$. Since we would like to determine the accuracy of each eigenmode (each k_z^i) and find the spurious ones, we need to formulate the conservation of momentum in the network characterized by $\{[\tilde{V}_i], [\tilde{I}_i]\}$. In order to formulate the conservation of momentum in this network, the matrix representations of $[\tilde{\alpha}]$, $[\tilde{\beta}]$ and $[\tilde{N}_i^2]$ in the eigenbasis are required. In this basis, $[k_z^i]$ is a diagonal matrix (as shown in (19)), and each column is dedicated to a specific k_z , thus the spurious one can be identified. According to the physical interpretation of TLF, the new representations denoted by $[\tilde{\alpha}], [\tilde{\beta}]$, and $[\tilde{N}_i^2]$ are obtained from the following equations in which $[P^i]$ is used to change the basis,

$$\begin{aligned} [\tilde{N}_i^2] &= [P^i]^{-1}[\tilde{N}_i^2][P^i], \\ [\tilde{\alpha}] &= [P^i]^{-1}[\tilde{\alpha}][P^i], \\ [\tilde{\beta}] &= [P^i]^{-1}[\tilde{\beta}][P^i]. \end{aligned} \quad (21)$$

Using the conservation of momentum, an error vector for the 1D gratings is defined by

$$[\epsilon_\kappa] = \text{Diag} \{ [\tilde{\alpha}]^2 + [\tilde{\beta}]^2 + [k_z^i]^2/k_0^2 - [\tilde{N}_i^2] \}, \quad (22)$$

where ‘Diag { }’ means diagonal elements of the square matrix. If the structure is uniform along y or x , then, $[\tilde{\beta}]$ or $[\tilde{\alpha}]$ will be a null matrix, respectively. Similarly, in the case of the 2D gratings, the error vector is defined by

$$\begin{aligned} [\epsilon_\kappa] &= \text{Diag} \left\{ \begin{bmatrix} [\tilde{\alpha}]^2 & 0 \\ 0 & [\tilde{\alpha}]^2 \end{bmatrix} + \begin{bmatrix} [\tilde{\beta}]^2 & 0 \\ 0 & [\tilde{\beta}]^2 \end{bmatrix} \right. \\ &\quad \left. + [k_z^i]^2 / k_0^2 - \begin{bmatrix} [\tilde{N}_i^2] & 0 \\ 0 & [\tilde{N}_i^2] \end{bmatrix} \right\}, \end{aligned} \quad (23)$$

where $0 = 0_{K \times K}$ is a null matrix. Now, it is easy to see that the farther the eigenvalue $k_{z\kappa}^i$ is from its true value, the larger the magnitude is of the corresponding element of the error vector. Therefore, using the magnitude of ϵ_κ , the computed modes can be sorted according to their degree of accuracy in a descending order, and by choosing a carefully selected threshold level, all modes that are above the threshold are identified as incorrect ones.

3.3. Suppressing the effect of spurious modes

Each column of $[P^i]$ and $[Q^i]$ (defined in (13) and (16)) corresponds to a particular transmission line in the network characterized by $[\tilde{V}_i(z)]$ and $[\tilde{I}_i(z)]$ representing a mode with a

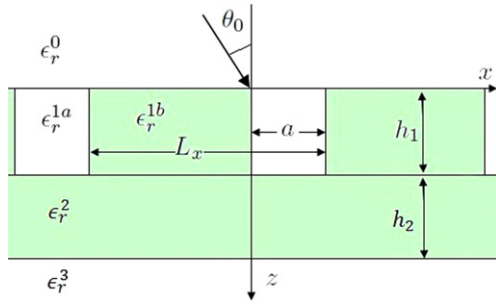


Figure 2. Planar two-layer structure containing a 1D metallic grating. $\epsilon_r^0 = \epsilon_r^3 = 1$, $\epsilon_r^2 = -100$, and the grating layer is made of $\epsilon_r^{1a} = 1$ and $\epsilon_r^{1b} = -100$. $L_x = 500$, $h_1 = h_2 = 500$ nm, and $\theta_0 = 30^\circ$.

propagation constant of k_z^i . Numerical artifacts that appear in the reflection coefficient are mainly due to real spurious modes and those that are near the real axis with small imaginary parts. Complex (or pure imaginary) spurious modes with large negative imaginary parts contribute very little to the input reflection coefficient. In the filtering mechanism introduced in [17], wave amplitudes of spurious modes were set directly to zero. However, in TLF, this would lead to zero voltage and current simultaneously, and the impedance matrix would cease to exist. Therefore, to diminish the effect of spurious modes that have small imaginary parts, we simply multiply their corresponding columns in the $[P^i]$ matrix by a small damping factor, e.g., 10^{-5} , and divide the associated rows in $[P^i]^{-1}$ by the same factor. Consequently, the voltage vectors (transverse electric fields) and the corresponding rows in the impedance matrix are divided by this small factor. This is equivalent to open circuiting those transmission lines associated with the spurious modes. In this way, the propagation of waves in the spurious transmission lines is prevented. Hence, the instabilities are removed while the power conservation is preserved. The criterion and approach that were proposed here can also be used in the FMM to determine the accuracy of the computed modes and to suppress the effect of the spurious ones.

4. Analysis of 1D gratings

4.1. Instability of TLF and identification of spurious modes

In this section, 1D metallic gratings with negligible loss are investigated. FMMs, such as TLF, are known to exhibit strong and unpredictable instabilities when used to analyze these structures in TM polarization. In order to further investigate the properties of spurious modes and to verify the correctness of the given criterion and the effectiveness of the procedure in removing instabilities, the grating structure in [11] is considered. This is shown in figure 2. In this structure, $\epsilon_r^0 = \epsilon_r^3 = 1$, $\epsilon_r^2 = -100$, and the grating layer is made of $\epsilon_r^{1a} = 1$ and $\epsilon_r^{1b} = -100$. The grating period is $L_x = 500$ nm, and the thicknesses of the layers are $h_1 = h_2 = 500$ nm. The angle of incidence of the TM polarized plane wave is $\theta_0 = 30^\circ$, and its wavelength is $\lambda = 632.8$ nm.

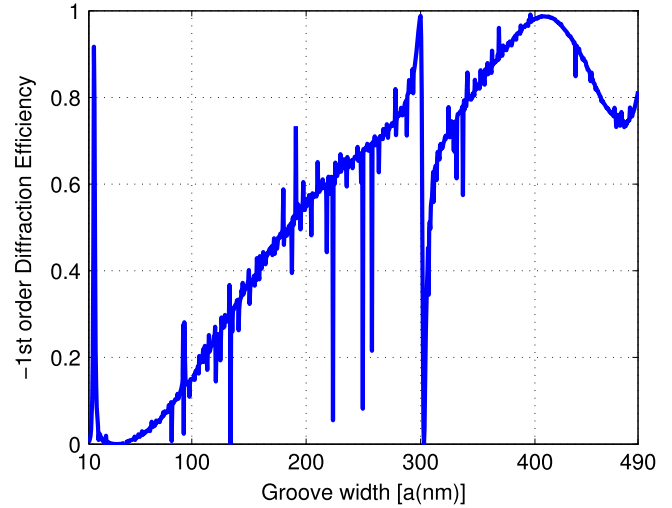


Figure 3. Minus-first-order diffraction efficiency of the structure shown in figure 2 versus the groove width. $\lambda = 632.8$ nm, $\theta_0 = 30^\circ$, and $M = 16$.

The minus-first-order diffraction efficiency, defined as the power of minus-first-order diffraction divided by the incident power, was computed using TLF for various groove widths a , and the results are shown in figure 3. This curve is obtained with a truncation order of $M = 16$ that requires a matrix of the size $(2M + 1) \times (2M + 1) = 33 \times 33$ to be diagonalized. As already shown in [11, 17], the TLF results exhibit unwanted fluctuations.

Comparing the normalized eigenvalues obtained using the TLF with those obtained from the exact modal method (EMM), we readily identify the spurious modes. Here, the EMM is used as the reference method in which, instead of the Fourier series of permittivity, the actual boundary conditions inside the binary grating are satisfied [22]. Although 1D metallic gratings can be treated accurately by this method, locating the complex roots of the resulting dispersion equation is usually a very difficult task that makes the EMM less attractive than the FMMs. Moreover, this method cannot be applied to 2D metallic gratings.

In figure 4, all 33 eigenvalues for a groove width of $a = 379$ nm and a truncation order of $M = 16$ are shown by the red +, and the modes that do not have an EMM counterpart are marked with blue circles. These modes are spurious ones that are the result of truncating the infinite matrices [17]. These incorrect modes cause instabilities in TLF. The spurious modes can be divided into two types: (i) those with normalized eigenvalues that are real or close to the real axis with values usually much larger than unity and (ii) those with complex or purely imaginary eigenvalues that usually appear with large imaginary parts. Furthermore, as mentioned in [17] spurious modes, unlike the correct ones, do not exhibit convergent behavior by increasing the truncation order. In table 1, values of k_z/k_0 that are real and represent propagation without attenuation computed by the EMM and TLF for $a = 379$ nm and $M = 16, 17$ are listed in an ascending order. Only two modes are correct, have EMM counterparts, and show convergent behavior. The others do not appear in the

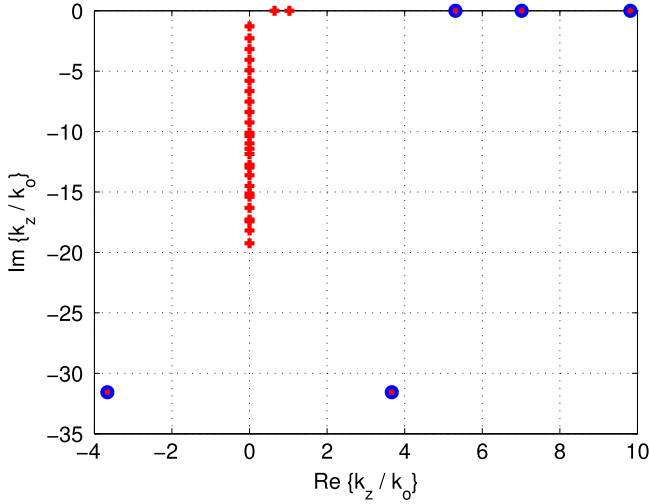


Figure 4. All eigenvalues are shown in red (+) , and the spurious ones are marked by blue circles for a groove width of $a = 379$ nm and $M = 16$.

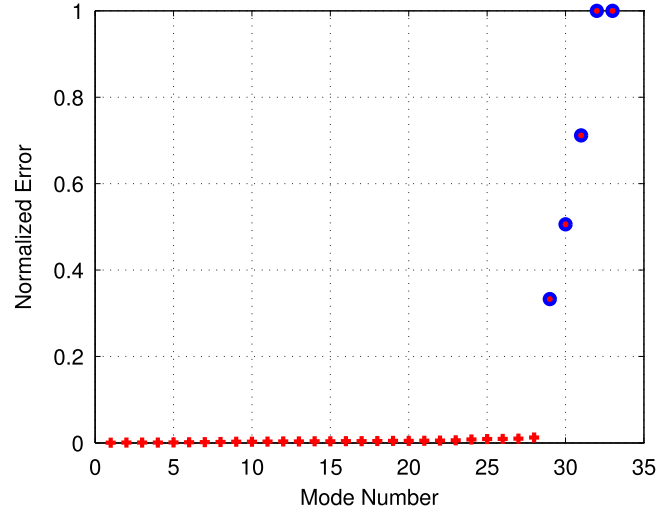


Figure 5. Normalized errors calculated by (22) for all modes. Spurious modes, marked with blue circles, correspond to the eigenvalues marked similarly in figure 4. The threshold level is 0.3 here.

Table 1. Normalized eigenvalues k_z^i/k_0 of modes that are real computed by the EMM and TLF for $a = 379$ nm.

EMM k_z^i/k_0	$M = 16$		$M = 17$	
	TLF k_z^i/k_0	Error	TLF k_z^i/k_0	Error
0.6432	0.6435	0.0061	0.6436	0.0073
1.0283	1.0286	0.0031	1.0285	0.0040
	5.3080	0.5059	5.9749	0.7262
	7.0143	0.7116	6.2630	0.7501
	9.8174	0.333	16.1631	1
			16.4949	0.8497

EMM and are unstable when the truncation order changes from 16 to 17. Also, note that the spurious modes have eigenvalues that are much larger than those of the true modes. The error values obtained from (22) for these modes are also shown in table 1. It is seen that the spurious modes show much larger errors than the correct ones.

Spurious modes with a complex or imaginary k_z also show unstable behavior, and their values change dramatically by increasing the truncation order. Such modes usually have large attenuation and contribute very little to the input reflection coefficient, so they do not cause instability. By means of the proposed error criterion, modes can be sorted in an ascending order according to their accuracy. As an example, error values for all 33 modes, normalized to the largest error and sorted in an increasing order, are shown in figure 5.

It should be emphasized that the main cause of the instabilities is the set of spurious modes whose eigenvalues are almost real because of their small or zero attenuation within the grating layer. Hence, the threshold level must be selected based on the smallest error in these modes. Usually, there is a noticeable gap between the errors of the correct and spurious modes as shown in figure 5. The amount of this abrupt variation determines the threshold level. All modes with an error larger than this threshold level are identified as

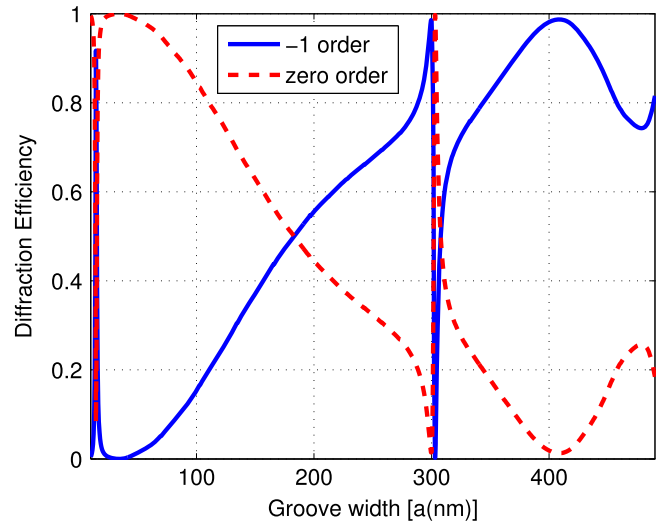


Figure 6. Minus-first- and zero-order diffraction efficiencies of the structure shown in figure 2 under TM^z polarization with $\lambda = 632.8$ nm and $\theta_0 = 30^\circ$ when the columns of $[P^i]$ related to the real-valued spurious modes are multiplied by 10^{-5} .

spurious modes. For example, according to error values in table 1 or figure 5, for $M = 16$, the threshold level must be smaller than 0.333 and larger than 0.0126.

4.2. Reducing the effect of spurious modes

The minus-first-order diffraction efficiency as a function of groove gap a for the structure shown in figure 2 was recomputed after applying the proposed method of removing instabilities. The result with a truncation order of $M = 16$ is shown in figure 6. Here, we multiply the columns of $[P^i]$ that related to the real-valued spurious modes by 10^{-5} and divide the corresponding rows in $[P^i]^{-1}$ by this number. The selected damping factor should be small enough to prevent flowing of energy in these modes and to suppress the effect of spurious

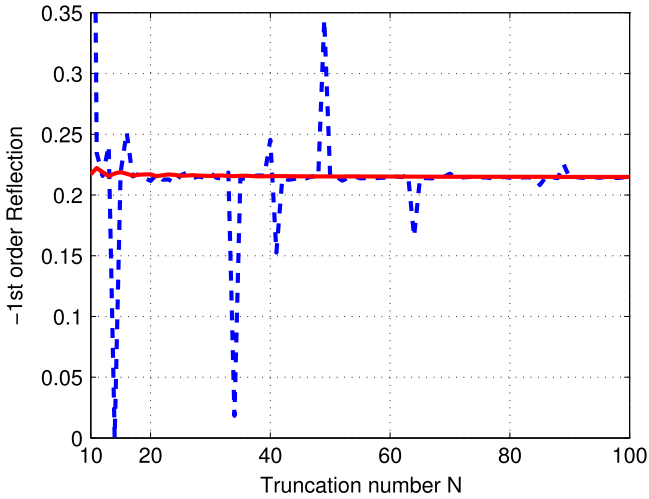


Figure 7. Convergence of minus-first-order diffraction efficiency as a function of the truncation order after (solid line) and before (dashed-dotted line) applying the proposed method. $a = 115$ nm, $\theta_0 = 30^\circ$, and $\lambda = 632.8$ nm.

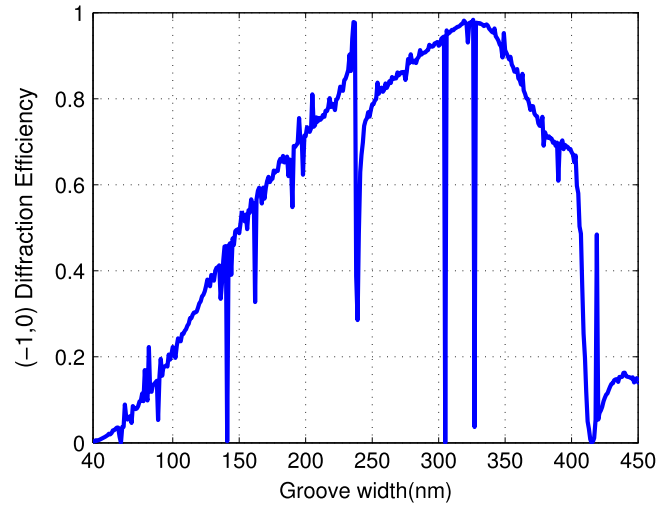


Figure 8. The $(-1, 0)$ order diffraction efficiency of the 2D periodic structure shown in figure 1 illuminated by a plane wave with a magnetic field parallel to the y axis and an electric field on the xz plane at $\lambda = 632.8$ nm and $\theta_0 = 60^\circ$.

modes. However, this factor should not be too small such that the matrix becomes near singular. Here the spurious modes with real eigenvalues are open circuited, while those with complex eigenvalues have not been altered. As shown in figure 6, all instabilities have been practically eliminated. In this structure, there is no transmission to the bottom layer, and only the minus-first- and zero-order diffraction efficiencies are nonzero. It is apparent from figure 6 that the sum of these two diffraction efficiencies is equal to 1, which shows that the conservation of power is satisfied.

In figure 7, the diffraction efficiency is shown versus the truncation order before and after applying the above elimination procedure to the real-valued spurious modes. It is observed that the convergence is also greatly improved. In the case of lossy metallic gratings, all spurious modes become lossy, and, consequently, numerical instabilities of the TLF are reduced naturally. However, low-loss plasmonic spurious modes still cause some numerical artifacts, especially, if the depth of the grating layer is small [17]. Therefore, applying the above elimination procedure to those spurious modes with small $|\text{Im}\{k_z\}|$ improves the convergence in the lossy case as well.

5. Analysis of 2D gratings

5.1. Instability of TLF and identification of spurious modes

In this section, 2D metallic gratings with negligible loss are studied. To explore the instabilities of the TLF in 2D gratings, the structure shown in figure 1 containing a rectangular grating is investigated. Parameters of the structure are $\epsilon_r^0 = \epsilon_r^3 = 1$ and $\epsilon_r^2 = -100$, and the grating layer is made of $\epsilon_r^{1a} = 1$ and $\epsilon_r^{1b} = -100$. The grating period is $L_x = L_y = 500$ nm, and the thicknesses of the layers are $h_1 = h_2 = 500$ nm. The magnetic field of the incident wave is parallel to the y axis, its electric field is on the xz plane, and the incident angle is $\theta_0 = 60^\circ$. The values of $(-1, 0)$ order

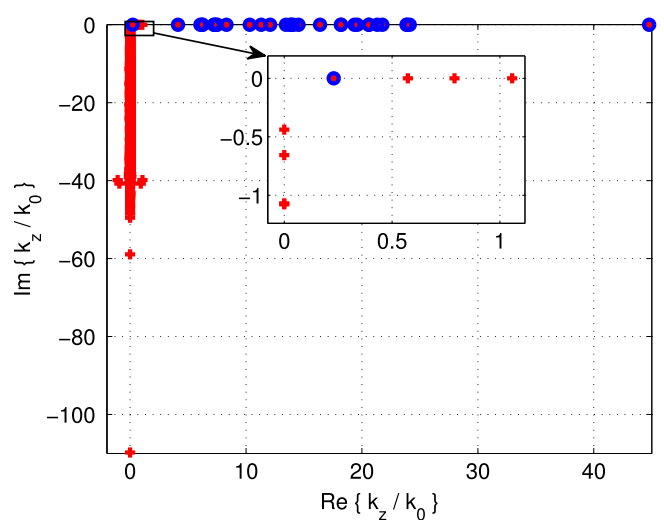


Figure 9. All normalized eigenvalues are shown by red (+), but only real-valued spurious modes are marked by blue circles ($a = 348$ nm and $M = N = 23$).

diffraction efficiency computed by means of the TLF as a function of the air gap is shown in figure 8. This curve is obtained with the truncation order of $M = N = 23$ (M is for the x and N is for the y direction) that requires a matrix of the size $2(2M + 1)^2 \times 2(2M + 1)^2 = 4418 \times 4418$ to be diagonalized. To speed up the computation, a more efficient formulation proposed in [23] for the symmetric structures is used. Here, the structure and the incident wave are both symmetric with respect to the $y = 0$ plane; hence, the dimension of the matrix is approximately halved.

Spurious modes can be detected by applying the error criterion given in (23) and by exploiting the fluctuating behavior of these modes with respect to the truncation order. In figure 9, distribution of the normalized eigenvalues on the complex k_z plane for a groove width of $a = 348$ nm with $M = N = 23$ are shown by the red +, but only real-valued

Table 2. Normalized eigenvalues k_z^i/k_0 of the few first modes that are real for $a = 348$ nm.

$M = N = 23$		$M = N = 24$	
k_z^i/k_0	Error	k_z^i/k_0	Error
0.2293	0.1967		
0.5736	0.0001	0.5810	0.0003
0.7899	0.0037	0.7835	0.0030
1.0570	0.0038	1.0490	0.0027
		3.8430	0.5623
4.1276	0.1294	3.9220	0.5600
6.0622	0.1137	6.3078	0.4214
6.2156	0.1241	6.6729	0.4562
6.2588	0.1262	6.9929	0.3919
7.2276	0.1316	7.5283	0.4091
7.2517	0.1357	8.2507	0.5299
7.4589	0.1207	8.2733	0.5339
7.4957	0.1222	9.0434	0.5253

spurious modes that cause numerical instability are marked by blue circles. As shown in figure 9, in contrast to the 1D grating, there also are spurious modes that have almost real eigenvalues with $k_z/k_0 < 1$, and they occur among the correct modes.

In table 2, normalized eigenvalues of the first few modes with purely real values that can propagate without attenuation are listed in an ascending order. We expect the correct modes to show convergent behavior and remain stable after changing the truncation order. Only three modes exhibit such behavior. Spurious modes, on the other hand, are unstable and wildly change when the truncation order increases by 1. Moreover, all spurious modes have larger amounts of errors than the correct ones.

Errors of real-valued eigenmodes are shown in figure 10 in which they are normalized to the maximum error of the computed modes and are sorted in an increasing order. Again, a large gap exists between the errors of correct modes and spurious ones that can be utilized to determine the threshold level. Numerical experiments show that, in most cases, this gap is considerable; however, in rare cases for which there is no clear gap, one can repeat the computation with a different truncation order, and usually a gap appears between the two sets of errors. Thus, by utilizing the gap in the error ε_{rc} , the correct modes with the smallest errors and the largest accuracy can be recognized.

The magnitude of the transverse magnetic field over one period is shown in figure 11 for a correct and a spurious mode. The spurious mode exhibits rapid oscillations, and its field has penetrated throughout the metal section that is incorrect. In fact, $k_p = \sqrt{\epsilon_r k_0^2 - (k_z^i)^2}$ becomes imaginary in the metal and dielectric sections, hence, the correct fields should show decaying behavior instead of oscillation.

5.2. Reducing the effect of spurious solutions

The $(-1, 0)$ order diffraction efficiency computed after multiplying the columns of $[P^i]$ related to the real-valued

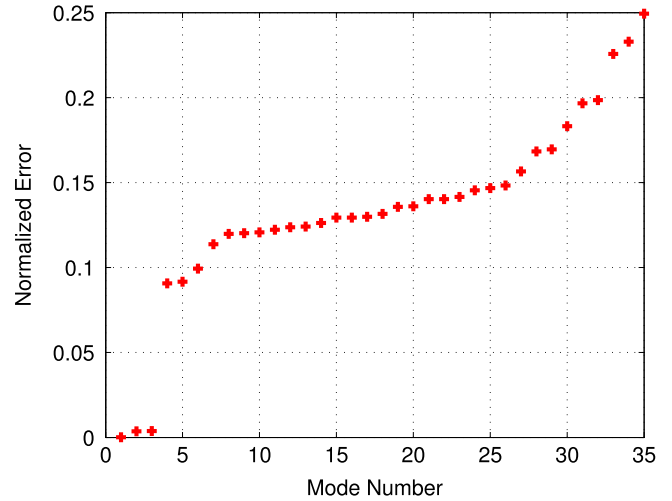
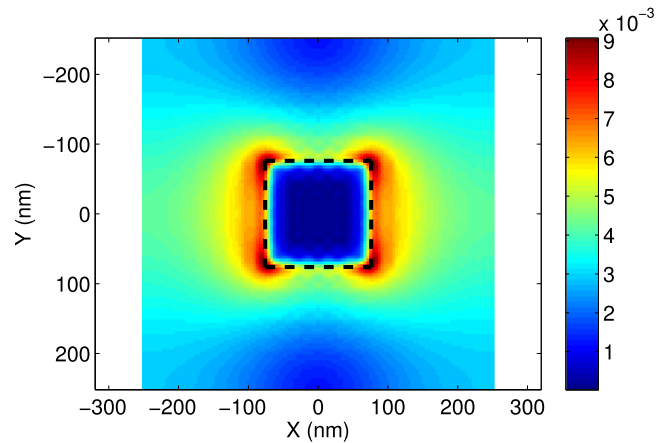
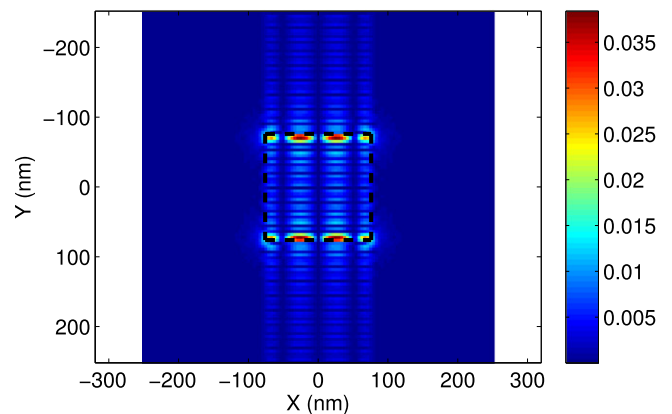


Figure 10. Normalized errors of real-valued eigenmodes computed by (23) for $a = 348$ nm and $M = N = 23$.



(a) Correct mode with $k_z/k_0 = 1.0570$



(b) Spurious mode with $k_z/k_0 = 4.1276$

Figure 11. Transverse magnetic field for a correct and a spurious mode.

spurious modes by 10^{-5} and dividing the corresponding rows in $[P^i]^{-1}$ by this number is shown in figure 12. This diagram is obtained with a truncation order of $M = N = 23$. Comparing with figure 8, we observe that, by using the proposed scheme,

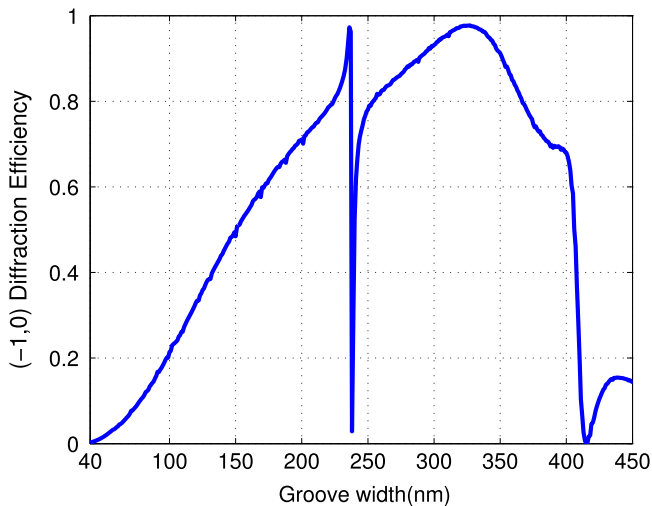


Figure 12. The $(-1, 0)$ order diffraction efficiency of the structure shown in figure 1 illuminated by a plane wave with its magnetic field parallel to the y axis and its electric field in the xz plane at $\lambda = 632.8$ nm and $\theta_0 = 60^\circ$ after multiplying the columns of $[P^i]$ related to the real incorrect modes by 10^{-5} .

numerical instabilities are greatly suppressed. The remaining small fluctuations can be attributed to those spurious eigenvalues that are very close to the correct ones. These spurious modes disturb the correct modes and, even after their elimination, instabilities do not disappear.

6. Conclusion

One-dimensional and 2D low-loss metallic gratings in TM polarization at optical frequencies were revisited. Numerical instabilities of the FM analysis of these structures are due to spurious modes. In this paper, a simple error criterion was proposed to sort the modes in the order of their accuracy to identify the unwanted modes. Moreover, a systematic method to suppress the effect of these spurious modes in the TLF formulation was presented. The proposed procedure does not violate the energy conservation.

Acknowledgments

We wish to acknowledge the Sheikh Bahaei National High Performance Computing Center at Isfahan University of Technology for performing the parallel computations on the RAKSH cluster.

References

- [1] Weiss T, Gippius N A, Tikhodeev S G, Granet G and Giessen H 2009 *J. Opt. A: Pure Appl. Opt.* **11** 114019
- [2] Tahmasebpour M, Bahrami M and Asgari A 2014 *Appl. Opt.* **53** 1449–58
- [3] D’Aguanno G, Mattiucci N, Bloemer M J, de Ceglia D, Vincenti M A and Alù A 2011 *J. Opt. Soc. Am. B* **28** 253–64
- [4] Deng L, Henning T, Klar P J, Feng S, Xie Z, Wang X, Sun W, Ye J, Han P and Zhang Y 2014 *J. Opt.* **16** 094015
- [5] Liu X, Zhao B and Zhang Z 2015 *J. Opt.* **17** 035004
- [6] Edee M K, Fenniche I, Granet G and Guizal B 2013 *Prog. Electromagn. Res.* **133** 17–35
- [7] Gaylord T and Moharam M G 1985 *Proc. IEEE* **73** 894–937 ISSN 0018–9219
- [8] Shahabadi M, Atakaramians S and Hojjat N 2004 *Science, Measurement and Technology, IEE Proceedings* **151** 327–34 ISSN 1350–2344
- [9] Tamir T and Zhang S 1996 *J. Lightwave Technol.* **14** 914–27 ISSN 0733–8724
- [10] Li L 1996 *J. Opt. Soc. Am. A* **13** 1870–6
- [11] Popov E, Chernov B, Nevière M and Bonod N 2004 *J. Opt. Soc. Am. A* **21** 199–206
- [12] Li L and Granet G 2011 *J. Opt. Soc. Am. A* **28** 738–46
- [13] Granet G 1999 *J. Opt. Soc. Am. A* **16** 2510–6
- [14] Guizal B, Yala H and Felbacq D 2009 *Opt. Lett.* **34** 2790–2
- [15] Granet G 2012 *J. Opt. Soc. Am. A* **29** 1843–5
- [16] Khavasi A, Mehrany K and Jazayeri A H 2008 *Opt. Lett.* **33** 159–61
- [17] Lyndin N M, Parriaux O and Tishchenko A V 2007 *J. Opt. Soc. Am. A* **24** 3781–8
- [18] Gundu K M and Mafi A 2010 *J. Opt. Soc. Am. A* **27** 1694–700
- [19] Gundu K M and Mafi A 2010 *J. Opt. Soc. Am. A* **27** 2375–80
- [20] Mei Y, Liu H and Zhong Y 2014 *J. Opt. Soc. Am. A* **31** 900–6
- [21] Li L 1997 *J. Opt. Soc. Am. A* **14** 2758–67
- [22] Foresti M, Menez L and Tishchenko A V 2006 *J. Opt. Soc. Am. A* **23** 2501–9
- [23] Zhou C and Li L 2004 *J. Opt. A: Pure Appl. Opt.* **6** 43